Structure
Article

Structure of the Dodecameric *Yersinia enterocolitica* Secretin YscC and Its Trypsin-Resistant Core

Julia Kowal,[1] Mohamed Chami,[1] Philippe Ringler,[1] Shirley A. Müller,[1] Mikhail Kudryashev,[1] Daniel Castaño-Díez,[1] Marlise Amstutz,[2] Guy R. Cornelis,[2] Henning Stahlberg,[1] and Andreas Engel[3,*]
[1]Center for Cellular Imaging and NanoAnalytics (C-CINA), Biozentrum, University Basel, Mattenstrasse 26, 4058 Basel, Switzerland
[2]Focal Area Infection Biology, Biozentrum, University of Basel, Klingelbergstrasse 50/70, 4056 Basel, Switzerland
[3]Department of Pharmacology, School of Medicine, Case Western Reserve University, Cleveland, OH 44106-4965, USA
*Correspondence: andreas.engel@case.edu
http://dx.doi.org/10.1016/j.str.2013.09.012

SUMMARY

The type III secretion system machinery, also known as the injectisome, delivers bacterial effector proteins into eukaryotic cells during infection. The outer membrane YscC secretin is a major part of *Yersinia enterocolitica*'s injectisome and is among the first components to assemble, solely assisted by its pilotin, YscW. We have determined the three-dimensional structures of the native complex and its protease-resistant core to 12 Å resolution by cryo-electron microscopy (cryo-EM) and show that YscC forms a dodecameric complex. Cryo-EM of YscC reconstituted into proteoliposomes defines the secretin's membrane-spanning region. Native YscC consists of an outer membrane ring connected via a thin cylindrical wall to a conical, periplasmic region that exposes N-terminal petals connected by flexible linkers. These petals harbor the binding site of YscD, a component of the inner membrane ring. A change in their orientation adapts the length of the YscC secretin and facilitates its interaction with YscD.

INTRODUCTION

During infection, pathogenic *Yersinia* (*Y. enterocolitica*, *Y. pseudotuberculosis*, and *Y. pestis*) transfer effector proteins into host target cells using the type III secretion system (T3SS), a macromolecular machinery composed of ~25 proteins that is called the injectisome (Cornelis, 2006; Kosarewicz et al., 2012). T3SSs have been identified in more than 25 different pathogens, including the genera *Yersinia*, *Pseudomonas*, *Shigella*, *Salmonella*, and *Escherichia*, and are essential for their virulence (Coburn et al., 2007). Of note, rhizobia exploit T3SSs to transfer effectors to their host for symbiotic purposes (Deakin and Broughton, 2009). Medium-resolution three-dimensional (3D) structures of *Salmonella* and *Shigella* T3SSs (Hodgkinson et al., 2009; Schraidt and Marlovits, 2011) and the *Shigella* needle (Fujii et al., 2012) have been determined by cryo-electron microscopy (cryo-EM), and an atomic model of *Shigella*'s needle has been established based on electron microscopy (EM) data, crystal or solution nuclear magnetic resonance subunit structures, and molecular modeling (Loquet et al., 2012). The recent refined model of the *Salmonella* basal body—an assembly composed of macromolecular rings that span the inner membrane (IM), the periplasmic space, and the outer membrane (OM)—provides further insight into the T3SS injectisome structure (Bergeron et al., 2013). These structural advances have been possible because *Salmonella* and *Shigella* produce stable injectisomes that can be purified and submitted to cryo-EM analyses. In stark contrast, the *Yersinia* injectisome is fragile and could only be observed in vivo by cryo-electron tomography (cryo-ET). This study revealed that the *Yersinia* basal body is a flexible structure that adapts its length during osmotic stress (Kudryashev et al., 2013).

During the invasion of host cells by bacteria, unfolded effector proteins are exported through the needle, which is anchored in the basal body. An alternative T3SS-dependent pathway involves an extracellular intermediate that can be reconstituted in vitro (Akopyan et al., 2011). In *Yersinia*, the IM ring is assembled from YscJ and YscD; the latter interacts with YscC (Ross and Plano, 2011) and is thought to partially bridge the periplasmic space (Spreter et al., 2009). YscC forms a ring in the OM (Burghout et al., 2004b), the secretin, which provides a channel for the injectisome needle.

Injectisome assembly has been shown to start in parallel from the OM and IM (Diepold et al., 2011). In the OM, assembly begins with YscC and proceeds inward through YscD and YscJ (Diepold et al., 2010). In parallel, the export apparatus (YscRSTUV) inserts into the IM, but assembly of the cytosolic part can only proceed when the IM ring has docked to YscC through YscD and YscJ (Diepold et al., 2011). The YscC secretin thus may be considered to be a platform for the injectisome assembly process.

Secretins are large, stable, homo-oligomeric OM protein complexes found in the type II secretion system (T2SS), the T3SS, the type IV pilus secretion system (T4P), and the filamentous phage extrusion machinery (Korotkov et al., 2011a). T2SS orthologs PulD (Chami et al., 2005), GspD (Korotkov et al., 2009; Reichow et al., 2010), and XcpQ (Bitter et al., 1998); T3SS orthologs EscC (Spreter et al., 2009), InvG (Kosarewicz et al., 2012; Marlovits et al., 2004; Schraidt and Marlovits, 2011), MxiD (Hodgkinson et al., 2009), and YscC (Koster et al., 1997); the T4P secretin PilQ (Berry et al., 2012; Burkhardt et al., 2011; Collins et al.,

2004; Jain et al., 2011); and the filamentous phage export machinery secretin pIV (Opalka et al., 2003) have been structurally characterized. C-terminal domains exhibit a high sequence homology across the secretins of different export systems, while N-terminal domains are only partially conserved (Genin and Boucher, 1994). Limited proteolysis experiments with the *Klebsiella oxytoca* T2SS PulD secretin revealed a C-terminal trypsin-resistant core, which participates in protein oligomerization and pore formation (Chami et al., 2005; Guilvout et al., 2006). The N-terminal GspD domain is involved in specific interactions with the IM protein GspC, the ortholog of the *Yersinia* IM protein YscD. The structure of the GspD-GspC interface from *Vibrio cholerae* defines 19 N-terminal residues of GspD that interact with 18 residues of GspC (Korotkov et al., 2011b). Such interactions have also been suggested for the N-terminal EscC region (Spreter et al., 2009) and were later confirmed by crosslinking studies (Sanowar et al., 2010). Moreover, the interaction of YscC with the YscD C terminus has been demonstrated by coimmunoprecipitation studies (Ross and Plano, 2011).

Several secretins have been observed through EM as purified solubilized single particles (Burkhardt et al., 2011; Chami et al., 2005; Opalka et al., 2003; Reichow et al., 2010; Spreter et al., 2009), as components of IM vesicles (Guilvout et al., 2006) and reconstituted proteoliposomes (Guilvout et al., 2008), and as low-diffracting two-dimensional crystals reconstituted in the presence of lipids (Collins et al., 2004). Secretins are reported to comprise 12–15 monomers. Embedded in the OM, they protrude into the periplasm, forming a large central pore. Comparison of 3D reconstructions obtained for the complexes formed by full-length PulD and its C-terminal domain allowed the N-terminal region to be defined (Chami et al., 2005). In addition, nanogold-labeling identified the N-terminal domain in pIV secretin (Opalka et al., 2003). Recent structural analyses revealed that the N-terminal domain of XcpQ forms dimers, promoting the hypothesis that secretins assemble as hexamers of dimers (Van der Meeren et al., 2013), which is supported by cysteine scanning mutagenesis of GspD and GspC protomers (Wang et al., 2012).

According to previous work, the *Y. enterocolitica* secretin assembles into an ~110 Å long, ~140 Å wide cylindrical complex with a stoichiometry that was tentatively postulated to be 13 (Burghout et al., 2004b). The discrepancy between this 13-fold symmetry of the OM ring and the prevalent 12-fold symmetry reported for a majority of secretins (Korotkov et al., 2011a) prompted us to determine the 3D structure of the YscC secretin by cryo-EM. We show that the YscC forms a dodecameric complex, compatible with its mass measured by scanning transmission electron microscopy (STEM). The 3D structures of the n-dodecyl-β-D-maltopyranoside (DDM)-solubilized YscC secretin and its protease-resistant core were determined to 12 Å and 13 Å resolution, respectively. Petals attached to the periplasmic side of the core by flexible linkers arise from the N-terminal YscC fragment lost during proteolysis. These N-terminal petals harbor the binding site for YscD, and the flexible linkers facilitate interaction with YscD. The petals also allow adaptation of the *Yersinia*'s basal body length under osmotic stress (Kudryashev et al., 2013). We demonstrate how YscC is embedded in a lipid bilayer, identifying its membrane-spanning region. Our results support the hypothesis that the YscC complex may act as the primary platform for the assembly of the *Y. enterocolitica* injectisome.

RESULTS

Expression, Purification, and Proteolysis of YscC Secretin Complexes

Native YscC was overexpressed in *Y. enterocolitica* E40 (pYV$^-$), and the intact secretin channels were purified to homogeneity from the membrane fraction (Figure 1); the purification protocol of Burghout et al. (2004b) was modified by the use of the low critical micelle concentration detergent DDM and extended by an additional purification step using size exclusion chromatography. The final gel filtration step allowed separation of the purified YscC into three different species: (1) unassembled native YscC monomers (64 kDa, elution volume, >17 ml), (2) secretin dimers (extrapolated mass: ~1.5 MDa, elution volume, <10.5 ml), and (3) the intact and highly pure single secretin rings (extrapolated mass: ~900 kDa, elution volume, 11.5 ml; Figure 1A), as confirmed by SDS-PAGE (Figure 1B) and cryo-EM of vitrified preparations (Figure 1C). Mass spectrometry (MS) showed the faint lower mass band on the silver-stained gel to arise from protein degradation during purification.

Incubating native YscC samples with trypsin before the final gel filtration step resulted in a complex that migrated at ~600 kDa (elution volume, 12.2 ml) on the subsequent Superose-6 filtration (Figure 1A). One intense and two very faint lower mass bands were obtained on SDS-PAGE analysis (Figure 1B). Cryo-EM confirmed the integrity of the proteolyzed complexes and documented the absence of a major protein domain (compare insets of Figures 1C and 1D).

MS and Edman degradation of native and proteolyzed YscC monomers running at 64 kDa and 32 kDa, respectively, on SDS-PAGE (Figure 1B) allowed the mass of the YscC core to be estimated and the fragments to be assigned to the YscC sequence (Figure S1 available online). Accordingly, proteolysis removed a 23.5 kDa region from the N terminus and an 8.8 kDa region from the C terminus of the native YscC (64.2 kDa), leaving a 31.9 kDa fragment that comprised Ile234-Arg526. MS analysis of the faint additional SDS-PAGE bands obtained after proteolysis (Figure 1B) showed that some of the cleaved N and C termini remained associated with the core complex during purification (Figure S2); from the relative band intensities, the amounts were ~25% for both the N- and C-terminal fragments.

Rotational Symmetry

To verify the previously reported 13-fold symmetry of the YscC complex (Burghout et al., 2004b), the rotational power spectra of 1,290 translationally centered top views of negatively stained proteolyzed YscC complexes were calculated and submitted to a neural network algorithm (Pascual-Montano et al., 2001, 2002) for classification of the rotationally unaligned particles. Figure S3A shows that only three class clusters exhibiting a distinct single major peak in the rotational power spectrum emerged, demonstrating that only symmetries of orders 9 (green), 10 (yellow), or 12 (red) were compatible with the data set, while neither 11 nor 13 were detected. Averages (Figure 2A) of particle subsets exhibiting distinct rotational power spectra were then

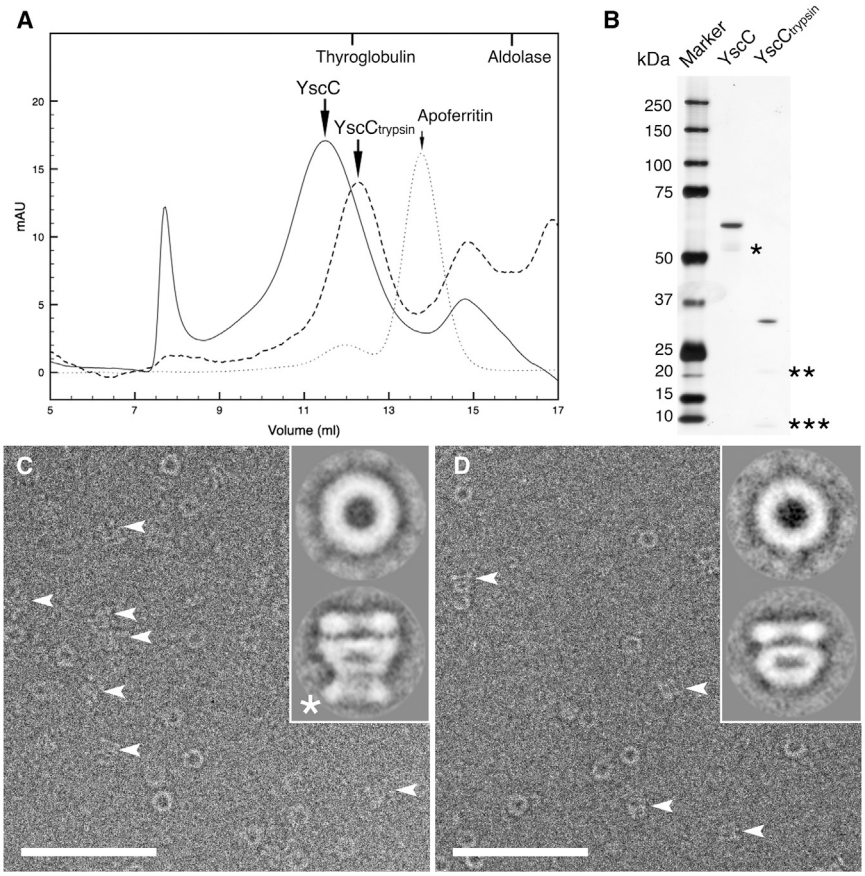

Figure 1. Purification and Cryo-EM of Native and Proteolyzed *Y. enterocolitica* YscC Secretins

(A) Size exclusion chromatography. The intact wild-type secretin eluted as an ~900 kDa species (arrow, YscC) and after proteolysis as an ~600 kDa species (arrow, YscC trypsin). The column was calibrated using thyroglobulin (670 kDa), apoferritin (440 kDa), and aldolase (158 kDa).

(B) Silver-stained SDS-PAGE of purified, phenol-treated (Hardie et al., 1996), native and proteolyzed secretins. The YscC monomers ran at 64 kDa and 32 kDa, respectively. As documented by MS, the fainter lower mass band in the native YscC lane (marked with an asterisk) arose from YscC degradation, while the very faint lower mass bands present after trypsin treatment (indicated by two and three asterisks) represent sparse N and C termini fragments that remained associated with the YscC core.

(C and D) Electron micrographs of vitrified native (C) and proteolyzed (D) YscC secretins, respectively. Insets, top and side view class averages, without applied symmetry. The particles appear as a single ring when viewed from the top and have a conical ladder-like structure when viewed from the side (arrowheads). Side views are shorter after proteolysis because the periplasmic petals (marked with an asterisk) are missing. Scale bars, 0.1 μm. Insets, 290 Å wide.

calculated starting with a reference bearing a "12 o'clock mark" (Figure 2C). The 12 o'clock mark was chosen to bootstrap the angular alignment of the YscC rings, preventing a bias for any particular rotational symmetry. During iterative refinement, averages of initially unaligned particles evolved to ring-shaped structures with clearly distinguishable subunits distributed according to the symmetry predicted by the neural network algorithm. These class averages exhibited identical diameters within the experimental error (Figure 2A). A principal-component analysis (Dube et al., 1993) executed with the Dynamo software (Castaño-Díez et al., 2012) on centered top views of negatively stained YscC cores belonging to the class cluster exhibiting 12-fold rotational symmetry revealed second and third eigenimages with distinct 12-fold symmetry (Figure 2B). This symmetry is accentuated in the rotational autocorrelation function (Figure S3B). Without preclassification, i.e., using all 1,290 top views, the 12 o'clock mark reference evolved to a ring-like structure with less distinct subunits (Figure 2D), exhibiting a major peak at order 12 and a secondary peak at order 9 in the rotational power spectrum (Figure 2E). Cryo-ET was carried out to ascertain the symmetry of liposome-embedded YscC complexes. In all, 282 subvolumes containing individual YscC complexes were iteratively aligned and averaged applying rotational symmetries ranging from C8 to C19 to the initial subvolume average. The average correlation coefficient between all subvolume averages and the nonsymmetrized final average structure from the entire data set plotted as a function of the imposed symmetry also indicates 12-fold symmetry (Figures S3C–S3E).

Multiple native and trypsinated YscC samples were imaged for mass measurement by STEM. Combining corresponding data sets (Figure S4) showed the mass of freeze-dried, unstained, DDM-solubilized secretin to be 899 ± 88 kDa (n = 1,177) and that of the proteolyzed complex to be 602 ± 83 kDa (n = 1,622). These two independent measurements allowed the number of subunits and the mass of bound detergent to be calculated. Accounting for the residual cleaved N- and C-terminal fragments that copurified with the trypsinated YscC complex (Table S1), the YscC secretin was found to be a dodecamer kept in solution by ~130 kDa or 254 molecules of firmly bound DDM.

Considering that symmetries 9 and 10 are highly improbable (Korotkov et al., 2011a) and that they would be compatible with neither the cryo-ET experiment nor the mass measurements, the symmetry of the YscC oligomer is most likely C12.

Cryo-EM of the Native and Proteolyzed YscC Secretins

In total, ~37,000 native and ~13,000 proteolyzed YscC particles were selected from electron micrographs and classified (Figures 1C and 1D; Supplemental Experimental Procedures). The characteristic class averages (Figure S5) showed native secretins to be 162 ± 5 Å wide and 182 ± 4 Å long (n = 10) and their proteolyzed counterparts only 148 ± 5 Å wide and 123 ± 4 Å long (n = 8).

In top views, both YscC complexes appear as ring-shaped particles (insets in Figures 1C and 1D). In side views, native particles exhibit three parts: (1) a compact ring, (2) a conical region,

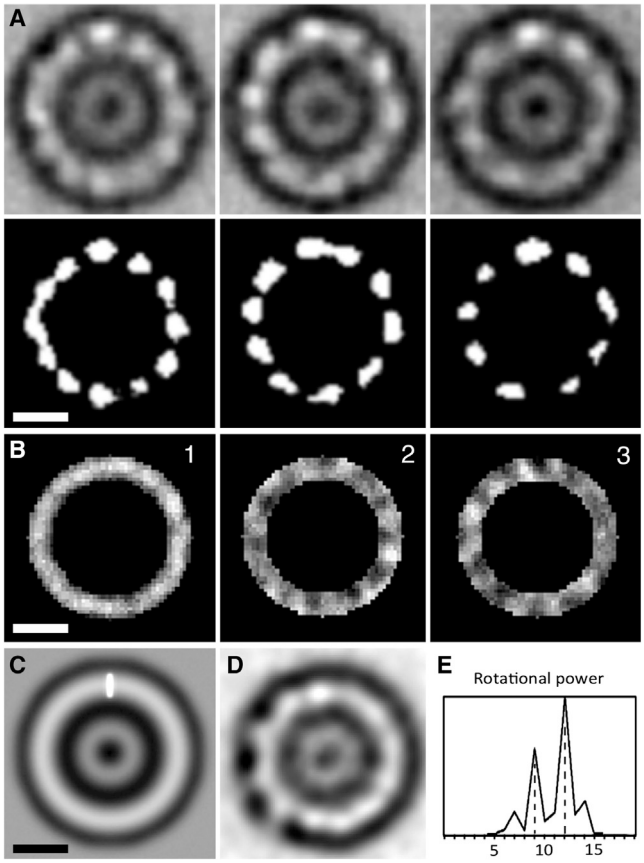

Figure 2. Rotational Symmetry of 1,290 Top-View Projections of Negatively Stained Protease-Resistant YscC Cores

(A) Correlation averaging of selected top-view projections. Rings classified into clusters according to their rotational power spectrum were iteratively aligned and averaged starting from a 12 o'clock mark reference shown later in (C). Averages were obtained after 100 iterations on the subsets with C12 symmetry (13% of all particles), C10 symmetry (13% of all particles), and C9 symmetry (14% of all particles). Bottom row depicts a binary segmentation of the gray scale images in the top row, facilitating identification of subunits.

(B) The eigenimages from 199 particles belonging to the cluster with C12 symmetry were calculated by the Dynamo package (Castaño-Díez et al., 2012). Eigenimages 2 and 3 reveal distinct 12-fold rotational symmetry.

(C) The "12 o'clock mark" reference was used to bootstrap the bias-free particle alignment.

(D) Correlation average from 1,290 particles, obtained after iterative alignment and averaging starting from the 12 o'clock mark reference shown in (C).

(E) Rotational power spectrum of (C) revealing the major peak at 12 and a secondary peak at 9.

and (3) elongated petals (Figure 1C, inset, indicated by an asterisk). Side views of the native complex (Figure S5A) show compact ring projections exhibiting a well-defined length of 167 ± 4 Å (n = 30). Two pronounced bands of density perpendicular to the cylinder axis appear on both sides of the conical part (Figure 1C, lower inset). The petals have a length of 58 ± 5 Å (n = 20) and a width of 32 ± 4 Å (n = 20), and they protrude from the conical region in different directions (Figure S5A), their orientation diverging by 25 ± 21° (n = 20) from the cylinder axis. A correlation average of petals (Figure S5A, inset) documents their elongated shape and the flexible linker (asterisk). Petals are missing in side views of proteolyzed YscC complexes (Figure 1D and Figure S5B).

To correlate our results from MS and Edman degradation with the loss of petals observed by cryo-EM, we used a multiple sequence alignment of prominent T2SS and T3SS secretins (Figure S6). Accordingly, the petals removed by proteolysis represent the N-terminal fragment (Figure S1), which harbors the binding site of YscD. Furthermore, the conical part of proteolyzed YscC complexes appears to have more rounded contours than its native counterpart.

Initial models of native and trypsinated, vitrified YscC complexes were calculated from class averages (Figure S5) imposing a C12 symmetry. The resulting density maps (Figure 3) of the native YscC complex emerged after seven refinement cycles, as demonstrated in Figure S5C. According to the Fourier shell correlation function between 3D maps from two independent data sets, the resolution of the native YscC map is 12 Å at a threshold of 0.143 and 15 Å at a threshold of 0.5 (Figure S7A) (Rosenthal and Henderson, 2003; see Experimental Procedures). The resolutions of the protease-resistant core are 13 Å and 15 Å according to the same criteria (Figure S7B).

Architecture of the YscC Secretin

The map of the native YscC complex (Figure 3A) has a length of ~165 Å and a diameter of ~165 Å (Figures 3D and 3E). Distinct regions are (1) the OM ring at the top, (2) the conical region in the middle, and (3) petals at the bottom that are removed by proteolysis. The first two regions form the ~120 Å high protease-resistant core (Figure 3C). The chamber within this core has inner diameters ranging from ~70 Å at both ends to ~85 Å in the middle, where the OM and conical part are linked by a thin-walled cylinder. The top view (Figure 3B) and the cross-section (Figure 3E) show that the native channel has two obstructions, one below the connection to the OM ring (periplasmic gate I, "plug") (Chami et al., 2005) and the other at the periplasmic end of the conical region (periplasmic gate II). The petals protruding from the conical part exhibit a lower density because of their orientational variability (Figure S8 and Movie S1) and were contoured separately (Supplemental Experimental Procedures).

The map of trypsin-cleaved YscC (Figure 3C) fits well into the 3D volume of the native YscC complex (Figure 3F). The protease-resistant core comprises the OM ring and the partially truncated conical part. Removal of 23.5 kDa from the N terminus and 8.8 kDa from the C terminus decreases the mass of the YscC complex by about one half, leaving an open cylinder devoid of petals (Figure 3F). The conical region of the proteolyzed YscC core has a smoother surface than the corresponding native region, lacking distinct protrusions close to the narrow connection to the OM ring.

To test the validity of the C12 symmetry derived from negatively stained YscC core particles and STEM mass measurements, we calculated maps from cryo-EM projections of native YscC secretins imposing C3, C4, and C6 symmetries. Figure S9 shows the remaining 12-fold symmetry elements after four refinement cycles in all cases. In addition, eight refinement cycles were accomplished, imposing C6 symmetry (Figure S9, bottom row, petals shown as mesh) to explore the possibility that the N-terminal domains might form dimers (Van der Meeren et al., 2013), but dimers could not be resolved.

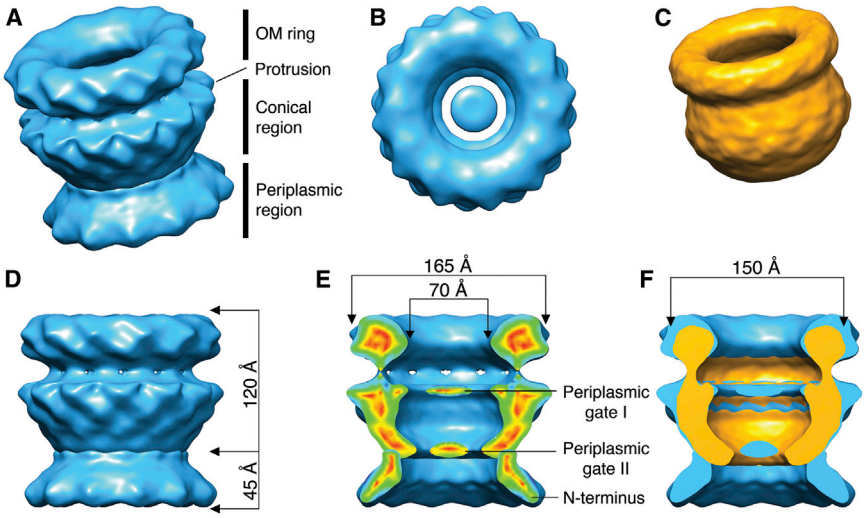

Figure 3. Cryo-EM Structure of the YscC Secretin

The 3D maps are isocontoured to include 100% of the mass of the C12 native and trypsin-cleaved YscC complexes.

(A) Tilted view of the native complex exhibiting the compact OM ring, the protrusion region, the conical region, and the periplasmic petals.

(B) Top view showing the extracellular surface and the gate closing the channel.

(C) Tilted view of the trypsin-cleaved YscC complex revealing major changes induced by proteolysis. The periplasmic petals have been removed, and the conical region has a less corrugated surface.

(D) Side view of (A).

(E) Axial section of the native YscC complex revealing a 70 Å channel closed by a first gate close to the OM ring and a second gate at the periplasmic end of the conical domain. Electron density is color coded from red to blue to indicate regions of stronger to weaker density.

(F) Axial section of the proteolyzed YscC (orange) is superimposed on the axial section of native YscC (blue).

The YscC Secretin in a Lipid Environment

OMs were isolated from the total membrane fraction, and SDS-PAGE and MS confirmed the presence of YscC. The intense high mass band on the gel shown in Figure 4A arose from YscC complexes and contained about 50% of the total protein. The strong band (labeled 2) at ~30 kDa (~20% content) arose from the porin OmpA. Negative stain EM of large vesicles and of membrane fragments up to ~1 μm wide (Figure 4B) revealed that the OM of *Y. enterocolitica* is densely packed with proteins; large complexes with the diameter of YscC are distributed in a "protein carpet." These complexes were also distinguishable in cryo-EM images of vitrified membranes (Figure 4C, arrowheads).

Purified secretins were reconstituted in the presence of *E. coli* polar lipids to explore their integration into the bilayer. Their periplasmic region was found to protrude toward either the inside or the outside of the vesicles (Figures 5A and 5B). A correlation average of 99 contrast transfer function (CTF)-corrected side views of vitrified YscC complexes integrated in proteoliposomes (Figure 5B) reveals that most of the OM ring and the narrow connection to the conical region are embedded in the membrane (Figures 5C and 5D).

DISCUSSION

Assisted only by its pilotin YscW (Burghout et al., 2004a), YscC assembles a stable, ring-like, multimeric, secretin complex at the beginning of injectisome morphogenesis (Diepold et al., 2010). It is, to date, the only membrane-bound complex of the *Yersinia* injectisome that has been isolated and submitted to structural and functional analyses (Burghout et al., 2004b). In spite of their sequence homology, secretins appear to comprise different numbers of subunits, with dodecameric complexes representing the majority (Korotkov et al., 2011a). High-resolution structural data for an entire secretin complex are still missing, but the structures of the N-terminal region of EscC of the T3SS (Spreter et al., 2009) and of InvG (Bergeron et al., 2013), GspD of the T2SS of enterotoxigenic *E. coli* (Korotkov et al., 2011a), and XcpQ from *Pseudomonas aeruginosa* (Van der Meeren et al., 2013)—all orthologs of YscC—were recently solved.

Identification and Characterization of the N-Terminal YscC Domain

We coexpressed YscC and the lipoprotein YscW in a *Y. enterocolitica* strain cured of its 70-kb pYV plasmid encoding the T3SS and purified the homooligomeric YscC according to the protocol described elsewhere (Burghout et al., 2004b). Two essential modifications yielded highly pure, aggregate-free preparations (Figure 1): (1) the use of the low-CMC detergent DDM to solubilize the OM, and (2) size exclusion chromatography to isolate the YscC oligomers. Trypsin was used to establish the protease-resistant YscC core; the cleaved fragments and the core peptide were identified by MS and Edman degradation (Figure S1). According to multiple sequence alignment of six different secretins, the identified YscC trypsin cleavage sites, Ile234 and Arg526 (Figure S6), correspond to the trypsin cleavage sites of *Klebsiella oxytoca* PulD (Gln262, Lys617) (Chami et al., 2005) and of *S. typhimurium* InvG (Lys269) (Spreter et al., 2009), confirming the equivalence of the C-terminal protease-resistant core of YscC and PulD/InvG and the similar overall structure of secretins (Korotkov et al., 2011a). Class averages of native (Figure S5A) and cleaved (Figure S5B) YscC—together with data from MS, Edman degradation, and multiple sequence alignment (Figure S6)—demonstrate that petals protruding from the conical region of native YscC into the periplasmic space correspond to the N-terminal domain where YscD docks (Ross and Plano, 2011), in agreement with recent models of the *S. typhimurium* injectisome (Spreter et al., 2009). Flexible connections anchoring these petals facilitate the assembly of the OM resident YscC with the IM ring formed early in injectisome morphogenesis by YscD-YscJ complexes (Diepold et al., 2011). The angular range that the petals assume (0–50°) and their length (58 ± 5 Å) suggest that the overall length of the YscC secretin can vary by 17 Å. This is an important functional feature

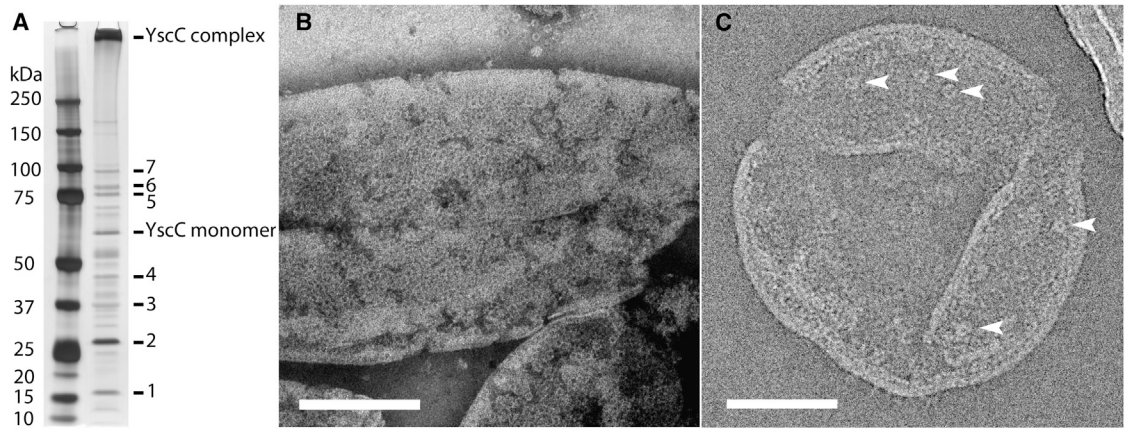

Figure 4. YscC in the Native *Y. enterocolitica* OM

(A) *Y. enterocolitica* OM Content. Silver-stained SDS-PAGE of purified OM. Main protein bands were identified by MS: 1, peptidoglycan-associated OM lipoprotein; 2, OmpA; 3, OmpC or OmpF; 4, ATP synthase beta subunit or putative Omp; 5, ferrichrome receptor FcuA; 6, OM protein assembly factor YaeT; 7, multidrug efflux protein. A gradient gel was used (NuPAGE 4%–12% Bis-Tris gel, with 2-[N-morpholino]ethanesulfonic acid-SDS) as running buffer.

(B) Electron micrograph of negatively stained *Y. enterocolitica* OM. Scale bar, 0.2 μm.

(C) Cryo-EM of the same membrane. Arrowheads, top views of YscC. Scale bar, 0.1 μm.

in view of the basal body length variations of the *Yersinia* injectisome recently observed with cryo-ET (Kudryashev et al., 2013).

The Symmetry of the YscC Secretin

Image processing of projections from negatively stained, trypsin-cleaved YscC complexes demonstrates the difficulty in determining the rotational symmetry of a secretin from projections of negatively stained samples (Figures 2 and S3). Using a neural network approach (Pascual-Montano et al., 2001) to classify rotational power spectra of centered top-view projections of YscC cores, we found that rings having distinct rotational symmetries of orders 9, 10, and 12 presented only 40% of the 1,290 projections inspected (Figure S3A). For 60% of the rings, the rotational power spectrum showed multiple peaks, indicating that rings had segments with different symmetries. The stability of the YscC complex requires YscC monomers to assemble tightly, suggesting that rings composed of nine monomers have different diameters than those built from 12 monomers. However, correlation averages of particle classes defined by rotational power spectra show that rings with different numbers of putative subunits all have the same diameter (Figure 2A). In addition, the OM ring diameter determined from side views of vitrified native YscC secretins (167 ± 4 Å) exhibits a small standard deviation (SD). This indicates that the oligomeric state of YscC is homogeneous but that negative stain artifacts produce rings of apparently different rotational symmetries.

Centered projections of the class cluster exhibiting a single peak of order 12 was submitted to a principal-component analysis, because this technique avoids the introduction of spurious symmetry components that may be generated when a data set is refined by cross-correlation against a template allowing rotational degrees of freedom (Dube et al., 1993) (Figures 2B and S3B). Introducing a 12 o'clock mark on a smooth reference ring yields a reference that does not allow different rotational degrees of freedom and, therefore, does not introduce a bias for a specific symmetry. The overall correlation average of all 1,290 top-view projections calculated using this reference produced a rotational power spectrum with a major peak at order 12 and a minor peak at order 9 (Figures 2C–2E).

We determined the mass of both native and cleaved YscC kept in solution by DDM by measuring the amount of electrons scattered by the freeze-dried particles. Considering the similarity of the native and the cleaved YscC cores (i.e., the OM ring and the conical region; Figure 3), we assume that both forms bind the same amount of DDM. The two independent mass values of the two YscC forms (Figure S4) exhibit SDs close to the theoretical value (Müller and Engel, 2006) and standard errors of the mean below the absolute accuracy of STEM mass measurements (±3%; Müller et al., 1992). As illustrated in Figure 1, some cleaved fragments remain bound to the protease-treated YscC complex during size exclusion chromatography. In fact, remnants of cleaved fragments are distinct in some class averages of proteolyzed YscC (Figure S5B). Taking these fragments into account (Table S1), the STEM data support the presence of 12 YscC subunits and ~130 kDa or 254 molecules of firmly bound DDM per complex.

Together, these results strongly suggest that YscC forms a dodecameric ring complex, in contrast to the previously proposed complex with C13 symmetry (Burghout et al., 2004b). Because the dodecameric form is further supported by the cryo-ET results for YscC secretins inserted in lipid vesicles (Figures S3C–S3E), we imposed C12 symmetry when refining the 3D map calculated from projections of vitrified complexes. Refinements with C3, C4, and C6 symmetries (Figure S9) demonstrate that the 12-fold features of the map persisted during four refinement cycles.

In view of the recent hypothesis that secretins may be hexamers of dimers (Van der Meeren et al., 2013), the refinement imposing C6 symmetry is of particular interest. The periplasmic petals are orthologs of the dimer-forming XcqP N-terminal domains (Van der Meeren et al., 2013) and may thus form dimers as well. Although the 12-fold structure of the YscC core remained conserved over four refinement cycles, the resolution

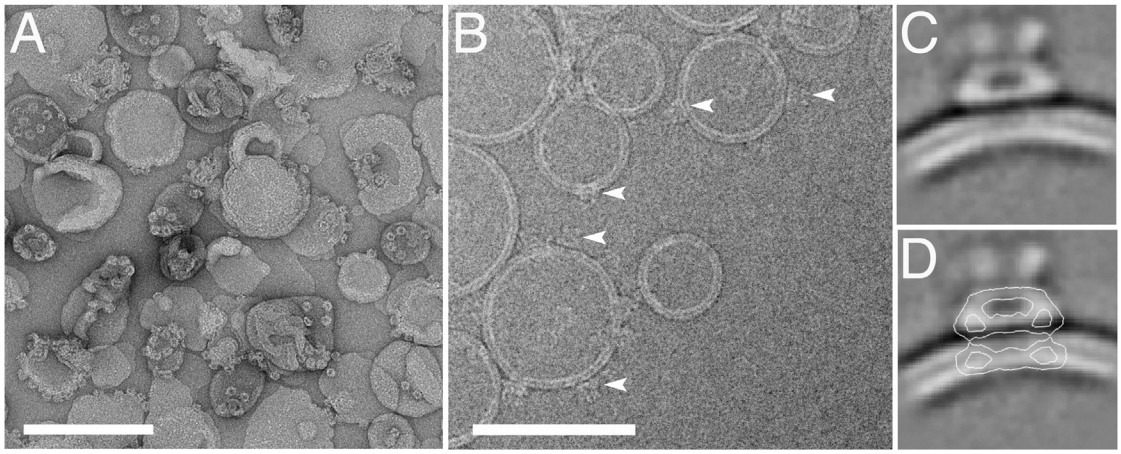

Figure 5. YscC Reconstituted into a Lipid Bilayer

(A) Electron micrograph of negatively stained YscC reconstituted into liposomes. Scale bar, 0.2 μm.

(B) Cryo-EM of YscC liposomes, shown in (A). Arrowheads, complexes viewed side on. Scale bar, 0.1 μm.

(C) Class average generated from 99 CTF-corrected side views of the YscC secretin reconstituted into the lipid bilayer.

(D) Contour of the calculated projection of the YscC map shown in Figure 3, superimposed on (C). The OM ring appears to be fully embedded in the lipid bilayer. Frame sizes of (C) and (D), 360 Å.

became worse and did not allow clear dimers of petals to be resolved (Figure S9C).

Features of the Native YscC and Its Protease-Resistant Core

Our 3D map of the YscC secretin exhibits a conduit with a minimum diameter of 70 Å. At an isocontour threshold compatible with the mass of 12 YscC monomers, two gates close the native channel. The more prominent gate is located at the periplasmic side of the conical region (periplasmic gate II), and the other one is located close to the OM ring (“plug”; Chami et al., 2005; periplasmic gate I) (Figures 3B and 3E). Both periplasmic gates persisted during refinements, but petals emerged only after four refinement cycles together with distinct surface features of the conical region (Figure S5C). Whereas gate I is found in all native T2SS and T3SS secretins, the YscC secretin also exhibits a second gate. Gates are crucial to prevent the loss of cellular contents during injectisome assembly. They must be flexible to facilitate release of effector proteins.

The periplasmic petals are lost upon trypsin treatment, but the protease-resistant core still exhibits similarities to the core of native YscC (Figures 3C and 3F), with the exception of the gates, which are lost during proteolysis. The thin-walled cylinder linking the OM ring and the conical region was previously suggested to represent the membrane-spanning region of PulD (Chami et al., 2005). However, according to class averages of reconstituted YscC secretin side views (Figures 5C and 5D), the compact OM ring is almost completely embedded in the membrane while the thinnest part of the cylinder wall localizes at the periplasmic lipid leaflet, supporting the earlier model of the pIV multimer in the context of the outer bacterial membrane (Opalka et al., 2003).

YscC Compared to Other Secretins

The high level of conservation between all secretin cores suggests that sequence-diverse, but topologically similar, proteins provide the common structure that drives the assembly of the OM rings and implies that they exhibit similar architectures and identical rotational symmetry. While a dodecameric arrangement has been reported for most secretins studied (Korotkov et al., 2011a), the 14-fold symmetry of the pIV and PilQ multimers (Jain et al., 2011; Opalka et al., 2003) and the 15-fold symmetry of InvG (Schraidt and Marlovits, 2011) represent exceptions. The subnanometer resolution of the *Salmonella* needle complex structure harboring the InvG secretin and the refined model of the *Salmonella* T3SS basal body (Bergeron et al., 2013) exclude doubts about its 15-fold symmetry.

Given the conservation of the secretin C-terminal cores that dictate the assembly process (Guilvout et al., 2006), secretins having different stoichiometries are expected to exhibit different diameters. However, the dimensions of the YscC core closely correspond to those of GspD (Reichow et al., 2010), PulD (Chami et al., 2005), MxiD (Hodgkinson et al., 2009), and InvG (Schraidt and Marlovits, 2011) (Figure 6). In contrast, the size of the periplasmic petals and the arrangement of the gates are different in YscC. Edman degradation and MS specify the mass of the petals (Figure S1), and sequence alignment reveals the differences between the N-terminal domains, which are 7.3 kDa larger in GspD and 3.3 kDa larger both in MxiD and InvG than in YscC (Figure S6), explaining the smaller size of the YscC petals. In PilQ from *Thermus thermophilus*, these extensions form a long cylindrical, periplasmic space-spanning structure by the packing of conserved α-β domains into rings, which could not easily adapt to changes of the periplasmic space under osmotic stress (Burkhardt et al., 2012). This packing arrangement is detailed by the model of *Salmonella*’s basal body (Bergeron et al., 2013) and is also indicated in the structure of the cholera toxin secretion channel (Reichow et al., 2010). We do not observe the packing of conserved α-β domains in the native YscC structure: the petals rather assume different orientations (Movie S1) and cannot form rings. While this flexibility facilitates adaptation of the basal body length to the periplasmic space under osmotic

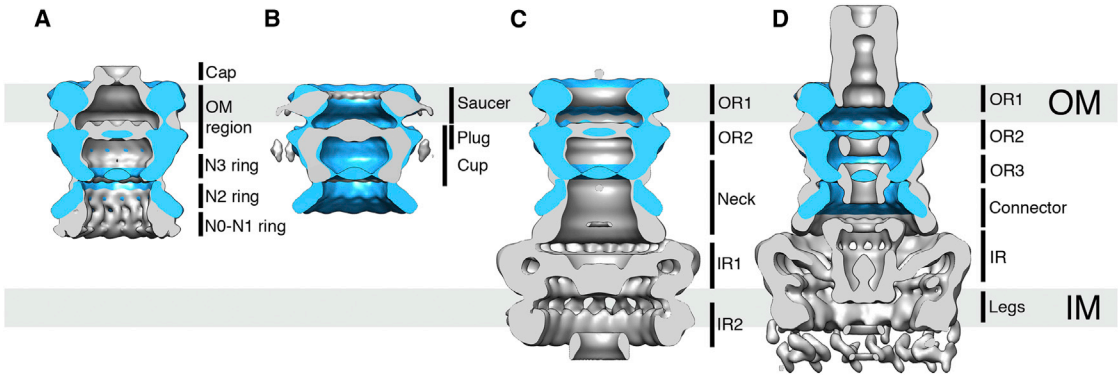

Figure 6. Comparison of the YscC Complex, in Blue, with Secretin Architectures, in Gray
(A) *V. cholerae* (secretin GspD [Reichow et al., 2010]; EMDB 1763).
(B) *K. oxytoca* (secretin PulD [Chami et al., 2005]).
(C) T3SS base complex of *S. typhimurium* in the closed state (secretin InvG [Schraidt and Marlovits, 2011]; EMDB 1214).
(D) T3SS needle complex of *S. flexneri* in the open state (secretin MxiD [Hodgkinson et al., 2009] EMDB 1617).

stress (Kudryashev et al., 2013), it imposes limitations in aligning the projections accurately.

GspD, PulD, MxiD, and InvG are open at the periplasmic end of the channel, where the major obstruction (periplasmic gate II) is found in YscC. GspD, PulD, and MxiD exhibit a massive gate close to the OM ring, where YscC has only a thin obstruction (periplasmic gate I). A higher resolution structure of YscC is needed to explain this discrepancy.

The phylogenetic tree of secretins (Figure S10) shows the evolutionary interrelations between these proteins. The primary sequence of YscC is more closely related to T3SS secretins InvG (*S. typhimurium*) and MxiD (*S. flexneri*) than to EscC (enteropathogenic *E. coli*). T2SS secretins PulD (*Klebsiella oxytoca*) and GspD (*Vibrio cholerae*) are located on the branch that is most distant from YscC. The large evolutionary distance between YscC and PulD/GspD sequences may explain the different size of their N-terminal domains.

YscC as a Primary Platform for Injectisome Assembly

Because it is very stable (Burghout et al., 2004b), a crucial initial assembly product (Diepold et al., 2010), and a prerequisite for anchoring the basal body in the peptidoglycan (Diepold et al., 2011), the YscC secretin could well serve as an injectisome assembly platform. Whereas injectisomes of *S. typhimurium* and *S. flexneri* and assembled IM components of *S. typhimurium* have been isolated and characterized by EM, the YscC injectisome has only been visualized in situ by cryo-ET (Kudryashev et al., 2013), and the assembly of its IM rings has only been monitored in situ by fluorescence microscopy (Diepold et al., 2011). Therefore, it is particularly difficult to elucidate the assembly pathway of the *Yersinia* injectisome.

Two assembly models have been proposed, one starting at the IM level and the other at the OM level (Kosarewicz et al., 2012). Evidence for the former model comes from IM rings formed by PrgH and PrgK visualized by EM (Kimbrough and Miller, 2000; reviewed in Kimbrough and Miller, 2002), from studies of the impact of export apparatus proteins on the formation of the injectisome basal body (Wagner et al., 2010), and by analogy to the assembly pathway of the flagellar basal body (Aizawa, 1996; Macnab, 2004). However, recent work has demonstrated that the stability of individually assembled PrgH/PrgK or InvG rings is greatly increased when all components are present, suggesting that the InvG secretin binding to IM ring components may promote polymerization and/or stabilization of both rings (Sanowar et al., 2010). This observation is compatible with the requirement of YscC for the stabilization of *Yersinia's* IM platform that binds to the secretin via YscD and YscJ (Diepold et al., 2011).

The data outlined earlier are compatible with both assembly pathways, although the stability of the YscC secretin suggests that, at least for *Yersinia*, the pathway starting at the OM is more favorable. Thus, the symmetry of YscC is likely to dictate the symmetry of the whole basal body. The dodecameric YscC ring is compatible with the 24-fold rotational symmetry of the related *S. typhimurium* and *S. flexneri* IM rings (Hodgkinson et al., 2009; Schraidt and Marlovits, 2011). It is also compatible with the 24-mer ring that has been built from the structure of YscD and a homology model of YscJ. This model satisfied constraints of the cryo-EM structure of the YscC injectisome (Kudryashev et al., 2013).

Our analysis of the YscC secretin in solution and in a lipid bilayer provides insights into the YscC structure and on the integration of YscC secretin in the OM. We propose that this dodecameric complex, which has been shown to initiate the injectisome assembly (Diepold et al., 2010), may dictate the overall symmetry of the T3SS injectisome. We have identified the N-terminal region that connects to YscD, which forms the link to the IM platform (Diepold et al., 2011). This N-terminal petal domain, which is lost on proteolytic cleavage, is connected to the YscC core by a flexible hinge, facilitating assembly of the OM and IM components of the injectisome and adaptation of the YscC length (Kudryashev et al., 2013).

The pathogenicity of *Yersinia* resulted in an unmatched devastation of the European human population in the 14th century. *Y. pestis*, responsible for the bubonic plague, has imposing abilities to overcome the mammalian host cell immune system and intensively multiply because of its pathogenic arsenal. Two closely related pathogens, *Y. enterocolitica* and

Y. pseudotuberculosis, responsible for gastroenteritis and eventually generalized infections share with *Y. pestis* the Yop virulon, the core of pathogenicity (Cornelis, 2000). The progress reported here is a step toward the full structural characterization of the functional T3SS injectisome used by pathogenic *Yersinia* to inject effector proteins into host target cells.

EXPERIMENTAL PROCEDURES

For a detailed description of the purification steps, trypsin treatment, reconstitution, cryo-EM, STEM, and image processing, see Supplemental Experimental Procedures.

YscC Expression, Purification, and Tryptic Digestion

The homooligomeric YscC was solubilized in DDM and purified according to the protocol described elsewhere (Burghout et al., 2004b). The last step of the purification separated the pure YscC oligomer from YscC oligomer dimers and small contaminants by gel filtration. One hundred micrograms of the purified YscC oligomer (0.1 mg/ml) was incubated with 1 μg/ml of N-p-tosyl-L-phenylalanine chloromethyl ketone-treated trypsin (Sigma). A control experiment without trypsin was performed.

Cryo-EM of the Native and Proteolyzed Complexes

Low-electron-dose images were recorded on Kodak SO163 film using a defocus range of 1,000–3,500 nm and subsequently digitized. The digitized images were then reduced to a resolution of 2 Å per pixel by 2 × 2 pixel.

Image Processing and Visualization

In all, 37,200 native and 13,000 proteolyzed YscC were processed. Models were refined imposing C12 symmetry until the resolution reached the best value. Various mask parameters were explored for native YscC to minimize the influence of flexible petals that impaired projection alignment. The density threshold for surface rendering (Chimera) was chosen to enclose the volume corresponding to molecular weights of 770 kDa for the native YscC complex, 282 kDa for the flexible petals of native YscC, and 384 kDa for the proteolyzed complex.

Symmetry Determination Using Negative Stain EM

A reference-free classification method, principal-component analysis, and a correlation averaging method based on an initial reference with a 12 o'clock mark were used.

Cryo-ET

Tomograms of liposomes containing YscC were recorded, manually aligned, and reconstructed by weighted back-projection. The symmetry of the liposome-embedded complexes was calculated by independent subvolume averaging.

STEM

The mass values of native and proteolytically cleaved YscC complexes solubilized in DDM were determined by measuring the amount of electrons scattered by single complexes using quantitative STEM.

Preparation and Imaging of *Y. enterocolitica* OM

OM fragments were collected and imaged by cryo-EM.

Reconstitution into Liposomes and Imaging

YscC was reconstituted into liposomes of *E. coli* polar lipids. Images were recorded by cryo-EM and processed.

ACCESSION NUMBERS

The following 3D structures have been deposited in the EMDataBank: YscC_core, EMD-5720; YscC_N terminus, EMD-5721; and YscC_trypsinized, EMD-5722.

SUPPLEMENTAL INFORMATION

Supplemental Information includes Supplemental Experimental Procedures, ten figures, one table, and one movie and can be found with this article online at http://dx.doi.org/10.1016/j.str.2013.09.012.

ACKNOWLEDGMENTS

The authors gratefully acknowledge the expert technical assistance of B. Anderson and K. Goldie. This work was supported by the Maurice Müller Foundation of Switzerland, the Swiss National Science Foundation (SNF 3100AOB-128659, SNF Sinergia CRSII3_125110, NCCR Structural Biology), and the Swiss Initiative for Systems Biology (SystemsX.ch). The work has been supported by grants from the Swiss Federal Government and the Maurice E. Mueller Foundation.

Received: July 30, 2013
Revised: September 4, 2013
Accepted: September 11, 2013
Published: October 24, 2013

REFERENCES

Aizawa, S.I. (1996). Flagellar assembly in Salmonella typhimurium. Mol. Microbiol. *19*, 1–5.

Akopyan, K., Edgren, T., Wang-Edgren, H., Rosqvist, R., Fahlgren, A., Wolf-Watz, H., and Fallman, M. (2011). Translocation of surface-localized effectors in type III secretion. Proc. Natl. Acad. Sci. USA *108*, 1639–1644.

Bergeron, J.R., Worrall, L.J., Sgourakis, N.G., DiMaio, F., Pfuetzner, R.A., Felise, H.B., Vuckovic, M., Yu, A.C., Miller, S.I., Baker, D., and Strynadka, N.C. (2013). A refined model of the prototypical Salmonella SPI-1 T3SS basal body reveals the molecular basis for its assembly. PLoS Pathog. *9*, e1003307.

Berry, J.L., Phelan, M.M., Collins, R.F., Adomavicius, T., Tønjum, T., Frye, S.A., Bird, L., Owens, R., Ford, R.C., Lian, L.Y., and Derrick, J.P. (2012). Structure and assembly of a trans-periplasmic channel for type IV pili in Neisseria meningitidis. PLoS Pathog. *8*, e1002923.

Bitter, W., Koster, M., Latijnhouwers, M., de Cock, H., and Tommassen, J. (1998). Formation of oligomeric rings by XcpQ and PilQ, which are involved in protein transport across the outer membrane of Pseudomonas aeruginosa. Mol. Microbiol. *27*, 209–219.

Burghout, P., Beckers, F., de Wit, E., van Boxtel, R., Cornelis, G.R., Tommassen, J., and Koster, M. (2004a). Role of the pilot protein YscW in the biogenesis of the YscC secretin in Yersinia enterocolitica. J. Bacteriol. *186*, 5366–5375.

Burghout, P., van Boxtel, R., Van Gelder, P., Ringler, P., Müller, S.A., Tommassen, J., and Koster, M. (2004b). Structure and electrophysiological properties of the YscC secretin from the type III secretion system of Yersinia enterocolitica. J. Bacteriol. *186*, 4645–4654.

Burkhardt, J., Vonck, J., and Averhoff, B. (2011). Structure and function of PilQ, a secretin of the DNA transporter from the thermophilic bacterium Thermus thermophilus HB27. J. Biol. Chem. *286*, 9977–9984.

Burkhardt, J., Vonck, J., Langer, J.D., Salzer, R., and Averhoff, B. (2012). Unusual N-terminal αααβββα fold of PilQ from Thermus thermophilus mediates ring formation and is essential for piliation. J. Biol. Chem. *287*, 8484–8494.

Castaño-Díez, D., Kudryashev, M., Arheit, M., and Stahlberg, H. (2012). Dynamo: a flexible, user-friendly development tool for subtomogram averaging of cryo-EM data in high-performance computing environments. J. Struct. Biol. *178*, 139–151.

Chami, M., Guilvout, I., Gregorini, M., Rémigy, H.W., Müller, S.A., Valerio, M., Engel, A., Pugsley, A.P., and Bayan, N. (2005). Structural insights into the secretin PulD and its trypsin-resistant core. J. Biol. Chem. *280*, 37732–37741.

Coburn, B., Sekirov, I., and Finlay, B.B. (2007). Type III secretion systems and disease. Clin. Microbiol. Rev. *20*, 535–549.

Collins, R.F., Frye, S.A., Kitmitto, A., Ford, R.C., Tønjum, T., and Derrick, J.P. (2004). Structure of the Neisseria meningitidis outer membrane PilQ secretin complex at 12 A resolution. J. Biol. Chem. *279*, 39750–39756.

Cornelis, G.R. (2000). Molecular and cell biology aspects of plague. Proc. Natl. Acad. Sci. USA *97*, 8778–8783.

Cornelis, G.R. (2006). The type III secretion injectisome. Nat. Rev. Microbiol. *4*, 811–825.

Deakin, W.J., and Broughton, W.J. (2009). Symbiotic use of pathogenic strategies: rhizobial protein secretion systems. Nat. Rev. Microbiol. *7*, 312–320.

Diepold, A., Amstutz, M., Abel, S., Sorg, I., Jenal, U., and Cornelis, G.R. (2010). Deciphering the assembly of the Yersinia type III secretion injectisome. EMBO J. *29*, 1928–1940.

Diepold, A., Wiesand, U., and Cornelis, G.R. (2011). The assembly of the export apparatus (YscR,S,T,U,V) of the Yersinia type III secretion apparatus occurs independently of other structural components and involves the formation of an YscV oligomer. Mol. Microbiol. *82*, 502–514.

Dube, P., Tavares, P., Lurz, R., and van Heel, M. (1993). The portal protein of bacteriophage SPP1: a DNA pump with 13-fold symmetry. EMBO J. *12*, 1303–1309.

Fujii, T., Cheung, M., Blanco, A., Kato, T., Blocker, A.J., and Namba, K. (2012). Structure of a type III secretion needle at 7-Å resolution provides insights into its assembly and signaling mechanisms. Proc. Natl. Acad. Sci. USA *109*, 4461–4466.

Genin, S., and Boucher, C.A. (1994). A superfamily of proteins involved in different secretion pathways in gram-negative bacteria: modular structure and specificity of the N-terminal domain. Mol. Gen. Genet. *243*, 112–118.

Guilvout, I., Chami, M., Engel, A., Pugsley, A.P., and Bayan, N. (2006). Bacterial outer membrane secretin PulD assembles and inserts into the inner membrane in the absence of its pilotin. EMBO J. *25*, 5241–5249.

Guilvout, I., Chami, M., Berrier, C., Ghazi, A., Engel, A., Pugsley, A.P., and Bayan, N. (2008). In vitro multimerization and membrane insertion of bacterial outer membrane secretin PulD. J. Mol. Biol. *382*, 13–23.

Hardie, K.R., Lory, S., and Pugsley, A.P. (1996). Insertion of an outer membrane protein in Escherichia coli requires a chaperone-like protein. EMBO J. *15*, 978–988.

Hodgkinson, J.L., Horsley, A., Stabat, D., Simon, M., Johnson, S., da Fonseca, P.C., Morris, E.P., Wall, J.S., Lea, S.M., and Blocker, A.J. (2009). Three-dimensional reconstruction of the Shigella T3SS transmembrane regions reveals 12-fold symmetry and novel features throughout. Nat. Struct. Mol. Biol. *16*, 477–485.

Jain, S., Mościcka, K.B., Bos, M.P., Pachulec, E., Stuart, M.C., Keegstra, W., Boekema, E.J., and van der Does, C. (2011). Structural characterization of outer membrane components of the type IV pili system in pathogenic Neisseria. PLoS ONE *6*, e16624.

Kimbrough, T.G., and Miller, S.I. (2000). Contribution of Salmonella typhimurium type III secretion components to needle complex formation. Proc. Natl. Acad. Sci. USA *97*, 11008–11013.

Kimbrough, T.G., and Miller, S.I. (2002). Assembly of the type III secretion needle complex of Salmonella typhimurium. Microbes Infect. *4*, 75–82.

Korotkov, K.V., Pardon, E., Steyaert, J., and Hol, W.G. (2009). Crystal structure of the N-terminal domain of the secretin GspD from ETEC determined with the assistance of a nanobody. Structure *17*, 255–265.

Korotkov, K.V., Gonen, T., and Hol, W.G. (2011a). Secretins: dynamic channels for protein transport across membranes. Trends Biochem. Sci. *36*, 433–443.

Korotkov, K.V., Johnson, T.L., Jobling, M.G., Pruneda, J., Pardon, E., Héroux, A., Turley, S., Steyaert, J., Holmes, R.K., Sandkvist, M., and Hol, W.G. (2011b). Structural and functional studies on the interaction of GspC and GspD in the type II secretion system. PLoS Pathog. *7*, e1002228.

Kosarewicz, A., Königsmaier, L., and Marlovits, T.C. (2012). The blueprint of the type-3 injectisome. Philos. Trans. R. Soc. Lond. B Biol. Sci. *367*, 1140–1154.

Koster, M., Bitter, W., de Cock, H., Allaoui, A., Cornelis, G.R., and Tommassen, J. (1997). The outer membrane component, YscC, of the Yop secretion machinery of Yersinia enterocolitica forms a ring-shaped multimeric complex. Mol. Microbiol. *26*, 789–797.

Kudryashev, M., Stenta, M., Schmelz, S., Amstutz, M., Wiesand, U., Castano-Diez, D., Degiacomi, M.T., Munnich, S., Bleck, C.K., Kowal, J., et al. (2013). In situ structural analysis of the Yersinia enterocolitica injectisome. eLife *2*, e00792.

Loquet, A., Sgourakis, N.G., Gupta, R., Giller, K., Riedel, D., Goosmann, C., Griesinger, C., Kolbe, M., Baker, D., Becker, S., and Lange, A. (2012). Atomic model of the type III secretion system needle. Nature *486*, 276–279.

Macnab, R.M. (2004). Type III flagellar protein export and flagellar assembly. Biochim. Biophys. Acta *1694*, 207–217.

Marlovits, T.C., Kubori, T., Sukhan, A., Thomas, D.R., Galán, J.E., and Unger, V.M. (2004). Structural insights into the assembly of the type III secretion needle complex. Science *306*, 1040–1042.

Müller, S.A., and Engel, A. (2006). Biological scanning transmission electron microscopy: imaging and single molecule mass determination. Chimia (Aarau) *60*, 749–753.

Müller, S.A., Goldie, K.N., Bürki, R., Häring, R., and Engel, A. (1992). Factors influencing the precision of quantitative scanning transmission electron microscopy. Ultramicroscopy *46*, 317–334.

Opalka, N., Beckmann, R., Boisset, N., Simon, M.N., Russel, M., and Darst, S.A. (2003). Structure of the filamentous phage pIV multimer by cryo-electron microscopy. J. Mol. Biol. *325*, 461–470.

Pascual-Montano, A., Donate, L.E., Valle, M., Bárcena, M., Pascual-Marqui, R.D., and Carazo, J.M. (2001). A novel neural network technique for analysis and classification of EM single-particle images. J. Struct. Biol. *133*, 233–245.

Pascual-Montano, A., Taylor, K.A., Winkler, H., Pascual-Marqui, R.D., and Carazo, J.M. (2002). Quantitative self-organizing maps for clustering electron tomograms. J. Struct. Biol. *138*, 114–122.

Reichow, S.L., Korotkov, K.V., Hol, W.G., and Gonen, T. (2010). Structure of the cholera toxin secretion channel in its closed state. Nat. Struct. Mol. Biol. *17*, 1226–1232.

Rosenthal, P.B., and Henderson, R. (2003). Optimal determination of particle orientation, absolute hand, and contrast loss in single-particle electron cryomicroscopy. J. Mol. Biol. *333*, 721–745.

Ross, J.A., and Plano, G.V. (2011). A C-terminal region of Yersinia pestis YscD binds the outer membrane secretin YscC. J. Bacteriol. *193*, 2276–2289.

Sanowar, S., Singh, P., Pfuetzner, R.A., André, I., Zheng, H., Spreter, T., Strynadka, N.C., Gonen, T., Baker, D., Goodlett, D.R., and Miller, S.I. (2010). Interactions of the transmembrane polymeric rings of the Salmonella enterica serovar Typhimurium type III secretion system. MBio *1*, pii: e00158-10.

Schraidt, O., and Marlovits, T.C. (2011). Three-dimensional model of Salmonella's needle complex at subnanometer resolution. Science *331*, 1192–1195.

Spreter, T., Yip, C.K., Sanowar, S., André, I., Kimbrough, T.G., Vuckovic, M., Pfuetzner, R.A., Deng, W., Yu, A.C., Finlay, B.B., et al. (2009). A conserved structural motif mediates formation of the periplasmic rings in the type III secretion system. Nat. Struct. Mol. Biol. *16*, 468–476.

Van der Meeren, R., Wen, Y., Van Gelder, P., Tommassen, J., Devreese, B., and Savvides, S.N. (2013). New insights into the assembly of bacterial secretins: structural studies of the periplasmic domain of XcpQ from Pseudomonas aeruginosa. J. Biol. Chem. *288*, 1214–1225.

Wagner, S., Königsmaier, L., Lara-Tejero, M., Lefebre, M., Marlovits, T.C., and Galán, J.E. (2010). Organization and coordinated assembly of the type III secretion export apparatus. Proc. Natl. Acad. Sci. USA *107*, 17745–17750.

Wang, X., Pineau, C., Gu, S., Guschinskaya, N., Pickersgill, R.W., and Shevchik, V.E. (2012). Cysteine scanning mutagenesis and disulfide mapping analysis of arrangement of GspC and GspD protomers within the type 2 secretion system. J. Biol. Chem. *287*, 19082–19093.